HHS Public Access

Author manuscript

Cell. Author manuscript; available in PMC 2016 August 13.

Published in final edited form as:

Cell. 2015 August 13; 162(4): 836–848. doi:10.1016/j.cell.2015.07.036.

A Conserved Bicycle Model for Circadian Clock Control of Membrane Excitability

Matthieu Flourakis[1], **Elzbieta Kula-Eversole**[1], **Alan L. Hutchison**[2], **Tae Hee Han**[1], **Kimberly Aranda**[3], **Devon L. Moose**[4], **Kevin P. White**[5], **Aaron R. Dinner**[2], **Bridget C. Lear**[4], **Dejian Ren**[3], **Casey O. Diekman**[6], **Indira M. Raman**[1], and **Ravi Allada**[1,*]

[1]Department of Neurobiology, Northwestern University, Evanston, IL, 60208

[2]Medical Scientist Training Program, James Franck Institute, Department of Chemistry, Institute for Biophysical Dynamics, University of Chicago, Chicago, IL, 60637

[3]Department of Biology, University of Pennsylvania, Philadelphia, PA, 19104

[4]Department of Biology, University of Iowa, Iowa City, IA, 52242

[5]Institute for Genomics and Systems Biology, University of Chicago, Chicago, IL, 60637

[6]Department of Mathematical Sciences, New Jersey Institute of Technology, Newark, NJ, 07102

Summary

Circadian clocks regulate membrane excitability in master pacemaker neurons to control daily rhythms of sleep and wake. Here we find that two distinctly timed electrical drives collaborate to impose rhythmicity on *Drosophila* clock neurons. In the morning, a voltage-independent sodium conductance *via* the NA/NALCN ion channel depolarizes these neurons. This current is driven by the rhythmic expression of NCA localization factor-1, linking the molecular clock to ion channel function. In the evening, basal potassium currents peak to silence clock neurons. Remarkably, daily antiphase cycles of sodium and potassium currents also drive mouse clock neuron rhythms. Thus, we reveal an evolutionarily ancient strategy for the neural mechanisms that govern daily sleep and wake.

*Correspondence to: r-allada@northwestern.edu.

Author Contributions

R.A., I.M.R. and M.F. designed the experiments; M.F. performed experiments and analyses related to Fig. 1, 2, 3, 4, 6 B-H, 7 A-G, S. 1, S.2, S.5C–D, S.6 and Tables S.1–2; E.K.E. designed, performed and analyzed experiments related to Fig 5, 6A–B, S.3, S.5A, S.5E and Tables S.3–4; A.L.H., K.P.W. and A.R.D. performed RNAseq analyses related to Fig 5A; C.O.D. developed the mathematical model related to Fig 7H–J and S.7; T.H.H performed electrophysiological recordings and analyses on lLNvs neurons related to Fig. S. 3, D.L.M. and B.C.L. performed experiments and analyses related Fig. S.5B; K.A. and D.R. generated the *NALCN*$^{fx/fx}$ mice; M.F. and R.A. wrote the manuscript; COD wrote sections related to the mathematical model. I.M.R. edited the manuscript.

Introduction

Circadian clocks have evolved to align organismal biochemistry, physiology and behavior to daily environmental oscillations. At the core of these clocks in all multicellular organisms are conserved transcriptional feedback loops (Allada and Chung, 2010; Hardin, 2011). In *Drosophila*, the bHLH-PAS transcription factor heterodimer CLOCK (CLK) and CYCLE (CYC) directly binds E-boxes (CACGTG) in target promoters of the clock genes, *period* (*per*) and *timeless* (*tim*), and activates their transcription. PER and TIM proteins feed back to repress CLK/CYC activity. The temporal separation of transcriptional activation and repression and/or mRNA and protein oscillations, in some cases by many hours (Lee et al., 1998), results in robust daily oscillations of *per*, *tim*, and other rhythmic transcripts. These molecular clocks in turn, control a broad range of cellular and physiological responses likely *via* the rhythmic transcription of clock output genes.

While molecular clocks are expressed in a variety of cell types, those in specific circadian clock neurons in the brain exhibit special properties. These so-called “master” circadian pacemakers, such as the mammalian suprachiasmatic nucleus (SCN) and the *Drosophila* lateral and dorsal neurons, drive robust 24-hour rhythms of sleep and wake behavior (Helfrich-Forster, 2005; Mohawk and Takahashi, 2011). Unlike generic clock cells, these clock neurons are interconnected *via* neural networks and as a result, produce coherent and sustained free running molecular and behavioral rhythmicity under constant conditions (Flourakis and Allada, 2015; Guo et al., 2014; Peng et al., 2003; Seluzicki et al., 2014; Shafer et al., 2002; Yang and Sehgal, 2001; Yao and Shafer, 2014). Although the anatomical features of brain pacemaker networks are highly divergent between mammals and invertebrates such as *Drosophila*, their ability to control sleep and wake cycles uniformly depends on daily rhythms of membrane excitability (Cao and Nitabach, 2008; Colwell, 2011; de Jeu et al., 1998; Kuhlman and McMahon, 2004; Sheeba et al., 2008). However, the mechanistic links between the molecular clock and the machinery controlling cellular excitability are not well understood.

Using patch-clamp analysis of the *Drosophila* DN1p, we show for the first time that circadian clock control of membrane excitability operates *via* resting sodium leak conductance through the NARROW ABDOMEN (NA) channel, providing timed depolarizing drive to circadian pacemaker neurons. We demonstrate that the sodium leak rhythm depends on rhythmic expression of NCA localization factor −1, linking the molecular clock and membrane excitability. We reveal that both flies and mice, separated by hundreds of millions of years in evolution, utilize antiphase oscillations of sodium and potassium conductances to drive clock control of membrane potential. Thus the conservation of clock mechanisms between invertebrates and vertebrates extends from core timing mechanisms to the control of membrane excitability in the master clock neurons governing sleep and wake.

Results

Rhythmic resting potassium and sodium leak currents collaborate to drive clock-controlled excitability of the *Drosophila* circadian neurons

To elucidate the mechanistic basis of daily changes in membrane excitability in *Drosophila* clock neurons, we performed whole-cell patch-clamp electrophysiology on the posterior dorsal neurons 1 (DN1p) on explanted brains (Flourakis and Allada, 2015; Seluzicki et al., 2014). DN1p neurons harbor molecular circadian clocks, and, under 12 hours light- 12 hours dark (LD) conditions, they contribute to increases in locomotor activity in advance of lights-on (i.e., morning anticipation) and lights-off (i.e., evening anticipation) (Zhang et al., 2010a; Zhang et al., 2010b). In addition to their established function in circadian behavior, the DN1p are an attractive target for patch clamp analysis as we can selectively label and identify DN1p neurons using the Clk4.1M-GAL4 driver in combination with UAS-CD8-GFP (Zhang et al., 2010a; Zhang et al., 2010b) (Fig. 1A). Furthermore, the DN1p neurons are easily accessible by electrode as they are located near the brain surface (Flourakis and Allada, 2015; Seluzicki et al., 2014).

Using whole-cell patch clamp analysis, a large daily variation in the firing frequency was detected (Fig. 1B, $p<0.05$ and Fig. S.1A). The wild type (*WT*) DN1ps fire at ∼10Hz in the morning (Zeitgeber Time, ZT0-4) and are nearly silent in the evening (ZT8–12) (Table S. 1A). The firing frequency in cell-attached configuration was comparable to that observed in whole-cell mode (Fig S.1B–D) suggesting that dialysis did not alter measurements of firing rates. The membrane potential also exhibited a temporal pattern: more depolarized in the morning than in the evening (Fig 1C, $p<0.05$ and Table S.1B). The neurons show daily rhythmic cellular excitability: more responsive to depolarizing currents in the morning than in the evening (Fig S.1E and Table S.2A). The input resistance had no significant diurnal rhythm (Fig.S.1F, Table S.1C). The rhythms in firing frequency and membrane potential were not evident in the arrhythmic core clock mutant per^{01}, indicating that the canonical clock controls daily changes in intrinsic membrane properties. Compared to *WT*, the per^{01} neurons are hyperpolarized (Fig. 1D), and show no rhythm in firing frequency (Fig. 1E, $p=0.41$), membrane potential (Fig. 1F, $p=0.66$) or cellular excitability (Fig S.2A, $p>0.41$). The per^{01} neurons also require more depolarizing current to fire at the same rates as *WT* (Fig. S.2B and table S.2B). Importantly, the high amplitude daily rhythm in firing frequency observed in *WT* neurons exceed those previously described in another set of *Drosophila* circadian neurons (LNvs) and more closely approximate those described in mammalian SCN clock neurons (Cao and Nitabach, 2008; Colwell, 2011; Kuhlman and McMahon, 2006; Park and Griffith, 2006; Schaap et al., 2003; Sheeba et al., 2008), indicating that DN1p analysis will be useful to define the mechanisms for clock control of membrane excitability. Given the role of the DN1p in morning and evening behaviors (Zhang et al., 2010a; Zhang et al., 2010b), these activity measurements suggest that DN1p activity in the morning can drive locomotor activity while the relative silence of the DN1p in the evening may have a permissive role on other cells controlling evening behavior.

To identify ionic conductances responsible for the resting membrane potential (RMP) rhythm, we blocked action potential firing using the voltage-dependent sodium channel

blocker, tetrodotoxin (TTX, 10μM), and then applied a cocktail of potassium (K) channel inhibitors (10mM TEA, 5mM 4AP, and 2mM CsCl) to block both voltage-dependent and voltage-independent (leak) K conductances (Fogle et al., 2011). We subsequently used N-Methyl-D-glucamine (NMDG) substitution of extracellular sodium to block sodium leak currents (Jackson et al., 2004; Lu et al., 2007; Raman et al., 2000) at different times of day. As in mammals (Kuhlman and McMahon, 2004) and mollusks (Michel et al., 1993), the effect of blocking K leak conductances in *Drosophila* was dependent on time-of-day, producing little change in the morning (Fig. 2A–B-D) but a sizable depolarization in the evening (Fig. 2C–D), indicating that rhythmic resting K conductance is conserved between flies and mammals (Kuhlman and McMahon, 2006). In contrast to K blockade, we discovered that blockade of resting sodium leak produced a larger hyperpolarization in the morning (Fig. 2A–B-E) than in the evening (Fig. 2C–E). Such time-of-day dependent effects of sodium channel blockade have not been previously reported. Notably, this time-of-day dependent effect on membrane potential of sodium blockade (Δ∼7 mV morning *vs* evening) is roughly equal to that of potassium blockade, suggesting that each makes a comparable contribution to daily excitability rhythms. As these rhythms are observed during network silencing from TTX, this suggests that changes in RMP are not driven by synaptic inputs but are intrinsic to the cells. Taken together, our results demonstrate that time-of-day-dependent sodium and K conductances, in the morning and evening, respectively, may underlie RMP rhythms.

The ion channel NARROW ABDOMEN controls *Drosophila* circadian pacemaker rhythms

A candidate mediator of resting sodium conductances in clock neurons and circadian behavior is the NARROW ABDOMEN (NA) ion channel (Lear et al., 2005; Nash et al., 2002). NALCN, the closely conserved mammalian homolog of NA, has been characterized as a voltage-independent mixed cation channel important for setting RMP and mediating resting leak sodium current (Lu et al., 2007; Swayne et al., 2009). This current is not blocked by TTX but can be reduced by either Gd^{3+} or replacement of extracellular sodium with NMDG (Lu et al., 2007). In a 12 hours light: 12 hours dark (LD) cycle, increases in locomotor activity in advance of lights-on (i.e., morning anticipation) and lights-off (i.e., evening anticipation) are suppressed in na^{har} mutants (Lear et al., 2005; Nash et al., 2002). Although NA expression in the DN1p can rescue morning and, to a lesser extent, evening phenotypes (Zhang et al., 2010a), it remains unclear whether NA is a rhythmic mediator of resting membrane potential of circadian clock neurons. We therefore examined clock neuron excitability in *na* mutant DN1p neurons. Strikingly, na^{har} mutant DN1p neurons were completely silent (Fig. 3A–B) and remained hyperpolarized throughout the whole day (Fig. 3C and table S.1B). No daily rhythm in cellular excitability was detected in na^{har} (Fig. 3D and Table S.2C; $p>0.35$). Positive current injections show that na^{har} mutant neurons fire fewer action potentials compared to controls, indicating that these neurons are healthy and can still generate action potentials but require more depolarizing current to fire at the same rate as *WT* neurons (Fig. 3D,E). Wild type membrane excitability can be restored by inducing NA expression only in the DN1p in the mutant, confirming that these effects are due to *na* and likely cell autonomous (Fig. 3E and Table S.2D). NMDG substitution induces an increase in the input resistance indicating that NA is open at rest (Fig. 3F).

We next directly measured voltage-clamped NA dependent current (I_{NA}) at different times of day. A voltage ramp protocol (from –113 mV to +87 mV) was used to measure the inward current at −113mV, in the presence of TTX. Replacing the sodium from the extracellular solution with NMDG reveals the sodium leak current (Fig. 4A). Consistent with the sodium leak current being driven specifically by NA, the observed current is reduced in the na^{har} mutant neurons and can be restored by rescuing the expression of NA in the mutant (Fig. 4A). Measuring I_{NA} at different times of day reveals a diurnal modulation of current density: it is higher in the morning and lower in the evening (Fig. 4B–C and table S.1D). No rhythm is detected in the na^{har} (Fig. 4B–C and table S.1D) or in per^{01} mutants (Fig. 4D, p=0.21), the latter indicating core clock control. Further, the rhythm in NA conductance was evident even after Clk4.1M-GAL4 driven rescue (Fig. 4E). Given GAL4 stability, any promoter driven transcriptional rhythms may not be evident as GAL4 protein rhythms and thus GAL4 induced transcription of *na* may not be rhythmic (Kaneko et al., 2000), suggesting that NA current rhythms do not require *na* transcript rhythms. Taken together these results indicate that the clock control of sodium leak current through NA mediates rhythms of resting membrane potential.

Nlf-1 expression is time-dependent and is required for locomotor activity rhythms and NA leak current

To identify molecular links between core clocks and membrane excitability, we employed fluorescence-activated cell sorting of GFP-labeled DN1p and performed RNA-Seq at distinct times during the LD cycle. Using empirical JTK_CYCLE (Hutchison et al., 2015), an updated version of JTK_CYCLE (Hughes et al., 2010), to detect rhythmic transcripts at a false discovery rate of 5% (Benjamini-Hochberg corrected $p<0.05$), we observed robust 24 h rhythms in CG33988, the fly ortholog of the NCA Localization Factor-1 (NLF-1) but not in *na* itself nor its regulatory subunits *unc79*, *unc80* (Lear et al., 2013) and NALCN-activators, Src family kinases (Lu et al., 2009), *Src42* and *Src64b* in flies (Fig. 5A). NLF-1 has been previously shown to interact with NA orthologs in worms (NCA-1 and −2) and mammals (Xie et al., 2013). NLF-1 protein is expressed in the endoplasmic reticulum and is required for the proper axonal localization of NCA-1 and −2 (Xie et al., 2013). Rhythmic expression of *CG33988/Nlf-1* transcript was further confirmed with quantitative PCR (Fig. 5B) and consistent with clock control, *CG33988/Nlf-1* transcript is rhythmic in the DN1p in constant darkness (DD) (Fig 5C). *Nlf-1* transcript is also highly enriched in the DN1p clock neurons in comparison to whole heads (Fig. 5D). Chromatin immunoprecipitation experiments indicate that the core clock transcription factor CLOCK rhythmically binds the *Nlf-1* genomic locus suggesting a direct biochemical link to the core clock (Abruzzi et al., 2011). Taken together, this suggests that *Nlf-1* is a key mediator of NA rhythms that couples the transcriptional oscillator to membrane potential rhythms.

To assess the function of NLF-1 in circadian behavior, we knocked down its transcript levels using three independent transgenic dsRNA and shRNA lines in combination with the broad circadian driver *tim*-GAL4. In contrast to the previously reported weak effect of CG33988 RNAi knockdown on evening behavior (Ghezzi et al., 2014), we found dramatic reductions in rhythmic strength in DD (3/3 lines) and reduced anticipation of lights-on (2/3 lines) and lights-off transitions (3/3 lines) under LD conditions (Fig. 6A, Fig. S.3). These effects are

comparable to those observed in loss-of-function *na* alleles (Lear et al., 2005) and knockdown of *na* using RNAi (Fig. S.3 and Tables S.3–4). Restricting *Nlf-1* knockdown to non-PDF clock neurons (*tim*-GAL4, *pdf*-GAL80) also caused reduced morning and evening anticipation as well as reduced rhythmicity (Tables S.3–4), consistent with prior *na* rescue studies (Lear et al., 2005). Further restricting *Nlf-1* knockdown to the DN1p using Clk4.1M–GAL4 resulted in reduced DD rhythmicity (Table S.3).

The role of *Nlf-1* extends to PDF neurons. Restricting *Nlf*-1 knockdown to PDF neurons, using two different *pdf*-GAL4 drivers (*pdf*-GAL4 and *pdf0.5*-GAL4 (Park et al., 2000), dramatically reduces free running rhythms (Table S.3), consistent with highly enriched *Nlf-1* transcript observed in larval PDF+ sLNv neurons (Nagoshi et al., 2010) and with the described role of NA in PDF neurons (Lear et al., 2005). In addition, we extended our patch clamp analysis to the large LNv neurons (Fig. S.4A). Here we observed clock-dependent rhythms in membrane properties as previously observed (Fig. S.4B–C) (Cao and Nitabach, 2008; Sheeba et al., 2008). In addition, we found clock-dependent NA current rhythms similar to those we observed for the DN1p with peak levels in the morning (Fig. S.4D). Thus our findings in DN1p extend to other circadian neurons.

We then tested whether *Nlf-1* is important for NA current levels, which may reflect the proper channel localization to the cell membrane. Knockdown of *Nlf-1* expression was confirmed in the DN1p with quantitative PCR (Fig. 6B). We find that knockdown in the DN1p results in a similar phenotype to that observed for *na* mutants with cells becoming hyperpolarized and silent (Fig. 6C). Cellular excitability is also decreased in the *Nlf-1* knockdown, as the neurons are less responsive to depolarizing currents (Fig. 6D and Table S.2E). NA-dependent current was also strongly suppressed after *Nlf-1* knockdown (Fig. 6E).

To further examine the mechanism by which NLF-1 might regulate NA, we assayed NA protein expression after *Nlf-1* knockdown. *Nlf-1* knockdown with a broad neuronal driver (elav-G4) also results in strong reductions in rhythmic strength in DD and reduced morning and evening anticipation (Fig. S.5A, Tables S.3–4). Surprisingly, NA protein levels were dramatically reduced in these flies (Fig. S.5B). We also observed lower NA expression (∼50% reduction) when *na* was driven transgenically in the DN1p of *Nlf-1* knockdown flies (Fig. S.5C–D). In part due to the small soma and limited expression in projections, we could not reliably assess cell membrane or axonal localization. Yet *Nlf-1* knockdown does not reduce DN1p *na* transcript levels (Fig. S.5E). *Nlf-1* knockdown in the DN1p phenocopies a *na* mutant suggesting NA current is nearly abolished (Fig. 6E) yet transgenic NA is reduced by just ∼50%. Thus, we favor the view that strong effects of *Nlf-1* knockdown on NA current are only in part due to changes in NA levels.

If the oscillation of *Nlf-1* transcript is critical to setting NA levels and DN1p membrane excitability, we would predict that *Nlf-1* overexpression would increase NA current at evening time points when NA current is typically at trough levels. We observed that in the evening (ZT8–12) NLF-1 overexpression depolarizes membrane potential, elevates firing rates (Fig. 6F) and cellular excitability (Fig. 6G and Table S.2.F), and, most importantly, increases NA current (Fig. 6H) at a time when each of those parameters is near their daily trough in wild-type flies. Indeed, sodium leak current density in the evening in *Nlf-1*

overexpression flies (~2pA.pF^{-1}) is comparable to that seen at peak levels in wild-type flies in the morning. Taken together, these results indicate *Nlf-1* expression is rhythmic and mediates NA activity rhythms. This demonstrates a molecular mechanism linking the core clock to membrane excitability *via* the rhythmic transcription of a factor important for ion channel function in *Drosophila* circadian neurons (Fig. 6I).

NALCN current is under clock control in mammalian SCN pacemaker neurons

Although we demonstrated a rhythmic function for resting sodium leak in *Drosophila* clock neurons, rhythmic resting sodium conductances have yet to be described in mammalian clock neurons. Previous patch clamp analyses of dissociated SCN neurons demonstrated the presence of a NALCN-like current (TTX-resistant, NMDG-sensitive, voltage-independent sodium conductance termed $I_{background}$) that is largely responsible for the initial phase of the depolarizing drive during the interspike interval (Jackson et al., 2004). To determine whether this activity is rhythmic in mammalian circadian pacemaker neurons, we performed voltage clamp analysis during subjective day and night from organotypic slices containing the SCN from mice entrained for two weeks in LD and then maintained under constant darkness conditions for at least three weeks. Rhythms in firing frequency, membrane potential and input resistance were observed, thus validating the preparation (Fig. S.6A–C). In the presence of TTX to block action potentials, the NALCN blockers, NMDG (Fig. 7A) or Gd^{3+} (Fig. S.6D), induce a hyperpolarization, while no additional effect of applying Gd^{3+} after sodium replacement with NMDG was observed (Fig. 7B). Importantly, in hippocampal neurons the vast majority of current with this pharmacological profile is mediated by NALCN (Lu et al., 2007).

To confirm the molecular identity of the sodium leak in the SCN, we generated a forebrain specific knockout of NALCN with a CamkIIα-cre driver. With this driver, CRE expression mimics the endogenous expression of *CamkIIα* (enriched in the forebrain, neuron specific (Casanova et al., 2001)). *CamkIIα* expression is also highly enriched in the SCN and loss of circadian rhythms in mice with a CamkIIα specific knockout of a core clock gene (*Bmal1*) is observed (Izumo et al., 2014). We first confirmed that the NMDG evoked hyperpolarization (Fig 7A) is greatly reduced in the *CamkIIα–Cre;NALCN*$^{fx/fx}$ animals compared to age-matched sibling controls (Fig. 7C–D, p=0.005). Consistent with a role of NALCN in controlling the membrane potential and firing frequency of neurons, *CamkIIα–Cre;NALCN*$^{fx/fx}$ SCN neurons were hyperpolarized and silent (Fig. S.6E–F, p<0.007). Importantly, a small depolarization current injected into the *CamkIIα–Cre;NALCN*$^{fx/fx}$ SCN neurons was able to evoke strong firing (Fig. S.7G) indicating that cells were healthy but required a greater depolarizing input to evoke action potentials. We further confirmed the presence of NALCN current during the interspike interval in organotypic slices containing the SCN with pharmacology: NMDG and Gd^{3+} sensitive. No additional block by Gd^{3+} was observed after NMDG application (Fig. S.6H–I). This NMDG sensitive inward current was greatly reduced in the *CamkIIα-Cre;NALCN*$^{fx/fx}$ SCN neurons (Fig. 7E–F, p=0.002). Taken together, these data indicate that the vast majority of the sodium leak flowing during the interspike interval in SCN neurons is carried by NALCN (I_{NALCN}) consistent with other mammalian neurons (Lu et al., 2007). We then assessed I_{NALCN} at different times of day

and found that it was significantly larger during the subjective day than subjective night consistent with a control by the circadian clock (Fig. 7G, $p<0.001$).

To determine the impact of a day-night change in I_{NALCN} (~0.7 pA.pF^{-1}) on firing frequency and membrane potential, we simulated sodium leak current modulation using an updated version of a mathematical model of SCN membrane excitability (Diekman et al., 2013) (see Experimental Procedures). This model accurately captures the effect of NALCN blockers on the membrane potential of SCN neurons (Fig. 7H). According to this model, modest daily changes in sodium leak conductance comparable to those observed experimentally can have sizable effects on neuronal firing rates (Fig. 7I). To explore the contributions of both sodium and potassium leak currents to the daily variation of firing rate in SCN neurons, we simulated concurrent modulation of these two conductances. Beginning from a subjective day firing rate of 7 Hz, reducing sodium leak conductance by the amount suggested by our experimental measurements (~0.7 pA.pF^{-1}, Fig. 7G) decreases firing rate to 2 Hz. Experimentally, we observed that during the subjective day, I_{NALCN} is, in fact, positively correlated with firing frequency (Fig. S.6J), suggesting that I_{NALCN} significantly impacts neuronal physiology. Even lower firing rates that are characteristic of subjective night (0.5 Hz) can be achieved by increasing potassium leak conductance in conjunction with this reduction in sodium leak (Fig. 7J, Fig. S.7). Thus, elevated sodium leak during the day and elevated potassium leak at night can recapitulate the experimentally observed daily variations in SCN firing rate through relatively modest changes in these leak currents.

Discussion

Taken together, our work defines a conserved mechanism for the maintenance of circadian oscillations necessary for robust daily behaviors (Fig. 6I) that we term the “bicycle” model. Membrane oscillations are driven by two cycles with opposite temporal phases analogous to cycling bicycle pedals. During the morning/day, sodium leak mediated by NA/NALCN is elevated while resting K currents are reduced depolarizing the neuron to promote elevated firing rates. During the evening/night, sodium leak is low and resting K currents are elevated, hyperpolarizing the cell to suppress firing rates. The clock-controlled transcript *Nlf-1* drives the rhythm of NA/NALCN current, linking the core clock to ion channel activity.

While *Drosophila* has been a well-established model for defining molecular genetic mechanisms, relatively little is known about the specific ionic currents that underlie fly pacemaker neuron excitability rhythms due to the small size of *Drosophila* soma. Most cellular electrophysiological analyses have focused on the largest cells, the large ventral lateral neurons (Cao and Nitabach, 2008; Fogle et al., 2015; Fogle et al., 2011; Sheeba et al., 2008). Yet, even in these neurons, the specific ionic currents under clock control have yet to be defined. Using whole cell patch clamp electrophysiology of DN1p pacemaker neurons, we found high amplitude oscillations of spontaneous firing rates and basal membrane potential that are comparable to those observed in mammalian SCN clock neurons. Moreover, we demonstrate clock control of both resting sodium leak conductance as well as resting potassium conductance. Our data suggest that the patch-clamp analysis of the DN1p

will be valuable in defining the ionic currents that mediate clock control of neuronal excitability.

Our data indicate that the daily changes in membrane excitability that we observe are cell autonomous. The observed cycles of resting currents are evident even in the presence of TTX. Bath application of TTX silences neurons and thus would block firing-dependent neurotransmitter release. Moreover, cycling sodium leak currents are driven by the transcriptional oscillation of *Nlf-1*, providing a cell autonomous mechanism for clock control. We propose that cell autonomous clock regulation collaborates with rhythmic network inputs, such as PDF, which likely act in the morning to excite DN1p neurons (Kunst et al., 2014; Seluzicki et al., 2014). In turn DN1p excitation drives waking behavior in the morning (Kunst et al., 2014; Zhang et al., 2010a; Zhang et al., 2010b) and free running rhythmicity, perhaps *via* the DH44 neurons in the pars intercerebralis (Cavanaugh et al., 2014). As the DN1p are also important for evening behavior (Zhang et al., 2010a), evening silencing may permit other neurons (e.g. the LNd) to drive evening behavior.

The clock control of membrane potential has largely focused on modulation of resting potassium conductance in the SCN (Kuhlman and McMahon, 2004) as well as in Bulla photoreceptors (Michel et al., 1993; Michel et al., 1999). Surprisingly, we observed rhythms of sodium leak conductance in the fly DN1ps and l-LNvs, as well as in mammalian SCN, that are mediated by the NA/NALCN channel. This sodium leak exhibits the pharmacological sensitivity previously defined for the NALCN current (Lu et al., 2007), most notably $NMDG^{+}$ and Gd^{3+} block. In addition, the current is reduced in *na* mutant fliesand in mice with a brain specific knockout of NALCN. Clock modulation of this sodium current also likely impacts neurophysiology. Loss of function *na* mutants and NALCN knockout result in silent and hyperpolarized neurons. Computational modeling of SCN neurons demonstrates that the modest daily rhythm of sodium leak can significantly impact overall firing rates. Thus our work defines a molecular mechanism for clock control of membrane excitability.

Using a combination of genomics, electrophysiology and behavior, our work reveals a molecular pathway that links the transcriptional clock to these sodium current rhythms. The mechanisms of clock control of membrane excitability have largely focused on the direct clock control of ion channel transcripts (Itri et al., 2005; Kudo et al., 2011; Meredith et al., 2006; Nahm et al., 2005; Pennartz et al., 2002; Pitts et al., 2006). Using RNA-seq and qPCR validation on FACS sorted DN1p neurons, we identify robust rhythms of *Nlf-1*, an ER protein that is important for the localization of NALCN and its orthologs (Xie et al., 2013). Moreover, RNAi knockdown of *Nlf-1* results in suppression of behavioral rhythms, NA expression and related current. Conversely, NLF-1 overexpression increases NA current, firing frequency and membrane potential in the evening when these parameters are typically at their troughs in wild-type flies, suggesting that *Nlf-1* controls activity and/or localization of NA. Chromatin immunoprecipitation has demonstrated rhythmic CLK binding at the *Nlf-1* locus (Abruzzi et al., 2011). Our cell-specific knockdown experiments indicate that *Nlf-1* functions broadly within the clock network to control morning and evening anticipation as well as DD rhythms, suggesting this mechanism is widely applied. Future work will be required to determine if *Nlf-1*/NA rhythms in morning and evening cells have

distinct phases. Nonetheless, we have defined a molecular pathway that directly links CLK-driven transcriptional oscillations to NA current and behavioral rhythms.

This mechanism may not only be operating in clock neurons but may be broadly involved in rhythmic changes in brain states. For instance, NALCN is critical to the maintenance of respiratory rhythms (Lu et al., 2007). Both fly and worm *na/nca* loss-of-function results in disrupted locomotion as well as altered sensitivity to general anesthetics (Humphrey et al., 2007). *na* mutant flies also show altered behavioral state transitions related to sleep and anesthesia (Joiner et al., 2013). More generally, the NA current here shows the identical electrophysiological profile to the tonic cation current required for regular firing in neurons of the mouse cerebellar nuclei (Raman et al., 2000).

Our work also demonstrates that, like the core molecular clock, clock control of membrane potential is also widely conserved in neurons important for sleep and wake. We hypothesize that the common ancestor of the mouse and the fly had master circadian pacemaker neurons that drove its daily behavior. Moreover, these clock neurons employed daily anti-phase sodium and potassium conductances to drive their rhythmic activity. Thus, our finding suggests an ancient strategy governing neuronal activity important for driving daily cycles of sleep and wake.

Experimental Procedures

Please see Supplemental Experimental procedures for detailed protocols.

Electrophysiological recordings from *Drosophila* neurons

Whole brain electrophysiology experiments were performed with pipettes (10–14 MΩ) filled with internal solution. The sodium leak current (I_{Na}) was examined in the presence of TTX (10μM), TEA (10mM), 4-AP (5mM) and CsCl (2mM), and was revealed by replacing the extracellular sodium with NMDG (Lu et al., 2007). All recordings were corrected for liquid junction potential (13mV). For analysis, cells with high series resistance or with low membrane resistance (<1GΩ) were discarded.

RNA isolation, amplification, and sequencing

RNA was isolated and amplified as previously described (Kula-Eversole et al., 2010). The quality and quantity of dsDNA was assessed on Bioanalyzer (Agilent). After quality control, libraries were generated using TruSeq Sample Preparation Guide (following manufacturer's protocol (Illumina)). The RNA-Seq was performed on HiSeq2000 (Illumina). Bowtie (Langmead et al., 2009) was used to align short-read aligner to references (obtained from flybase.org). Quantification was performed using eXpress (Roberts et al., 2011). Rhythmic transcripts were detected using empirical JTK_CYCLE (Hutchison et al., 2015), transcripts were considered robustly rhythmic when the Benjamini-Hochberg corrected p value or false discovery rate<0.05. Empirical JTK_CYCLE derives p values empirically considering asymmetric waveforms.

Mathematical modeling

Simulations of a Hodgkin-Huxley type model of SCN membrane excitability were performed using MATLAB R2012b (Mathworks, Natick, MA, USA). The model was fit to experimental data from SCN neurons and consists of a system of ordinary differential equations for membrane potential (*V*) and six ionic gating variables (*m*, *h*, *n*, *r*, *f*, and *b*):

$$\begin{aligned} C\frac{dV}{dt} &= I_{app} - I_{Na} - I_K - I_{Ca} - I_{BK} - I_{Cl} - I_{Kleak} - I_{NALCN} \\ &= I_{app} - g_{Na}m^3h(V - E_{Na}) - g_K n^4(V - E_K) - g_{Ca}rf(V - E_{Ca}) \\ &\quad - g_{BK}b(V - E_K) - g_{Cl}(V - E_{Cl}) - g_{Kleak}(V - E_K) - g_{NALCN}(V - E_{NALCN}) \end{aligned}$$

$$\frac{dx}{dt} = \frac{x_\infty(V) - x}{\tau_x(V)} \quad x = m, h, n, r, f, b$$

$$\begin{aligned} m_\infty &= \frac{1}{1+\exp(-(V+35.2)/8.1)}, & h_\infty &= \frac{1}{1+\exp((V+62)/4)}, \\ n_\infty &= \frac{1}{(1+\exp((V-14)/(-17)))^{0.25}}, & r_\infty &= \frac{1}{1+\exp(-(V+25)/7.5)}, \\ f_\infty &= \frac{1}{1+\exp((V+260)/65)}, & b_\infty &= \frac{1}{1+\exp(-(V+20)/2)}, \\ \tau_m &= \exp(-(V+286)/160), & \tau_h &= 0.51+\exp(-(V+26.6)/7.1), \\ \tau_n &= \exp(-(V-67)/68), & \tau_r &= 3.1, \\ \tau_f &= \exp(-(V-444)/220), & \tau_b &= 50 \end{aligned}$$

with parameter values C=5.7 pF, I_{app}=0 pA, g_{Na}=229 nS, g_K=14 nS, g_{Ca}=65 nS, g_{BK}=10 nS, g_{Cl}=0.3 nS, $g_{K\text{-}leak}$=0.04 nS, E_{Na}=45 mV, E_K=−97 mV, E_{Ca}=64 mV, E_{Cl}=−60 mV, and E_{NALCN}=−20 mV.

Our SCN model extends previously published versions (Diekman and Forger, 2009; Sim and Forger, 2007) by separating the leak current into sodium, potassium, and chloride components (with parameter values chosen based on our measurements of sodium leak current density and RMP), and incorporating a large-conductance calcium-activated potassium (BK) current. BK channels are voltage and calcium-gated. However, since the nanodomain calcium concentration sensed by the channel reaches equilibrium very quickly, we follow (Tomaiuolo et al., 2012) and model the gating as a purely voltage-dependent process. The differential equations were solved using the Euler-Maruyama method, with a time step of 0.01ms and standard Gaussian distributed voltage noise (μ=0, σ=0.5).

Supplementary Material

Refer to Web version on PubMed Central for supplementary material.

Acknowledgments

We thank B. White and H-S. Li for communicating results prior to publication, M. Vitaterna, K. Shimomura, A. Para, E. Zaharieva, D. Wokosin, C. Olker, Jordan I. Robson for technical assistance, J. Gu, R. Scott and B. White for the cloning and generation of UAS-NA^{HA} flies, Dr. Jean Richa (Transgenic and Chimera Mouse Facility at the

University of Pennsylvania) for ES cell injection and M. Gallio for reagents and comments on a draft of the manuscript. We also thank Bloomington *Drosophila* stock center, the National Institute of Genetics (NIG), Vienna *Drosophila* RNAi center (VDRC) for reagents and the TRiP at Harvard Medical School (NIH/NIGMS R01-GM084947) for providing transgenic RNAi fly stocks This work was supported by National Institutes of Health (NIH) grants R01NS052903 (to R.A), NS055293 and NS074257 (to D.R.), R00GM080107 (to B.C.L.), National Science Foundation (NSF) Division of Mathematical Science grant (DMS1412877 to C.O.D). This effort was in part sponsored by the Defense Advanced Research Projects Agency (DARPA) (D12AP00023, to R.A.); the content of the information does not necessarily reflect the position or the policy of the government, and no official endorsement should be inferred. This work was also supported by the Northwestern University Flow Cytometry Facility, by a Cancer Center Support Grant (NCI CA060553).The two photon microscope was supported by NINDS (NS054850). A.L.H. is a trainee of the NIH Medical Scientist Training program at the University of Chicago (NIGMS T32GM07281). This work made use of the Open Science Data Cloud (OSDC), which is an Open Cloud Consortium (OCC)-sponsored project. This work was supported in part by grants from Gordon and Betty Moore Foundation, the NSF and major contributions from OCC members like the University of Chicago. Our work is in memory of Howard Nash who re-discovered *narrow abdomen* and inspired our pursuit of studies of this channel.

References

Abruzzi KC, Rodriguez J, Menet JS, Desrochers J, Zadina A, Luo W, Tkachev S, Rosbash M. Drosophila CLOCK target gene characterization: implications for circadian tissue-specific gene expression. Genes & development. 2011; 25:2374–2386. [PubMed: 22085964]

Allada R, Chung BY. Circadian organization of behavior and physiology in Drosophila. Annual review of physiology. 2010; 72:605–624.

Cao G, Nitabach MN. Circadian control of membrane excitability in Drosophila melanogaster lateral ventral clock neurons. J Neurosci. 2008; 28:6493–6501. [PubMed: 18562620]

Casanova E, Fehsenfeld S, Mantamadiotis T, Lemberger T, Greiner E, Stewart AF, Schutz G. A CamKIIalpha iCre BAC allows brain-specific gene inactivation. Genesis. 2001; 31:37–42. [PubMed: 11668676]

Cavanaugh DJ, Geratowski JD, Wooltorton JR, Spaethling JM, Hector CE, Zheng X, Johnson EC, Eberwine JH, Sehgal A. Identification of a circadian output circuit for rest:activity rhythms in Drosophila. Cell. 2014; 157:689–701. [PubMed: 24766812]

Colwell CS. Linking neural activity and molecular oscillations in the SCN. Nature reviews Neuroscience. 2011; 12:553–569. [PubMed: 21886186]

de Jeu M, Hermes M, Pennartz C. Circadian modulation of membrane properties in slices of rat suprachiasmatic nucleus. Neuroreport. 1998; 9:3725–3729. [PubMed: 9858386]

Diekman CO, Belle MD, Irwin RP, Allen CN, Piggins HD, Forger DB. Causes and consequences of hyperexcitation in central clock neurons. PLoS computational biology. 2013; 9:e1003196. [PubMed: 23990770]

Diekman CO, Forger DB. Clustering predicted by an electrophysiological model of the suprachiasmatic nucleus. J Biol Rhythms. 2009; 24:322–333. [PubMed: 19625734]

Flourakis M, Allada R. Patch-clamp electrophysiology in Drosophila circadian pacemaker neurons. Methods in enzymology. 2015; 552:23–44. [PubMed: 25707271]

Fogle KJ, Baik LS, Houl JH, Tran TT, Roberts L, Dahm NA, Cao Y, Zhou M, Holmes TC. CRYPTOCHROME-mediated phototransduction by modulation of the potassium ion channel beta-subunit redox sensor. Proceedings of the National Academy of Sciences of the United States of America. 2015; 112:2245–2250. [PubMed: 25646452]

Fogle KJ, Parson KG, Dahm NA, Holmes TC. CRYPTOCHROME is a blue-light sensor that regulates neuronal firing rate. Science. 2011; 331:1409–1413. [PubMed: 21385718]

Ghezzi A, Liebeskind BJ, Thompson A, Atkinson NS, Zakon HH. Ancient association between cation leak channels and Mid1 proteins is conserved in fungi and animals. Frontiers in molecular neuroscience. 2014; 7:15. [PubMed: 24639627]

Guo F, Cerullo I, Chen X, Rosbash M. PDF neuron firing phase-shifts key circadian activity neurons in Drosophila. eLife. 2014:3.

Hardin PE. Molecular genetic analysis of circadian timekeeping in Drosophila. Advances in genetics. 2011; 74:141–173. [PubMed: 21924977]

Helfrich-Forster C. Neurobiology of the fruit fly's circadian clock. Genes, brain, and behavior. 2005; 4:65–76.

Hughes ME, Hogenesch JB, Kornacker K. JTK_CYCLE: an efficient nonparametric algorithm for detecting rhythmic components in genome-scale data sets. J Biol Rhythms. 2010; 25:372–380. [PubMed: 20876817]

Humphrey JA, Hamming KS, Thacker CM, Scott RL, Sedensky MM, Snutch TP, Morgan PG, Nash HA. A putative cation channel and its novel regulator: cross-species conservation of effects on general anesthesia. Curr Biol. 2007; 17:624–629. [PubMed: 17350263]

Hutchison AL, Maienschein-Cline M, Chiang AH, Tabei SM, Gudjonson H, Bahroos N, Allada R, Dinner AR. Improved statistical methods enable greater sensitivity in rhythm detection for genome-wide data. PLoS computational biology. 2015; 11:e1004094. [PubMed: 25793520]

Itri JN, Michel S, Vansteensel MJ, Meijer JH, Colwell CS. Fast delayed rectifier potassium current is required for circadian neural activity. Nature neuroscience. 2005; 8:650–656. [PubMed: 15852012]

Izumo M, Pejchal M, Schook AC, Lange RP, Walisser JA, Sato TR, Wang X, Bradfield CA, Takahashi JS. Differential effects of light and feeding on circadian organization of peripheral clocks in a forebrain Bmal1 mutant. eLife. 2014:3.

Jackson AC, Yao GL, Bean BP. Mechanism of spontaneous firing in dorsomedial suprachiasmatic nucleus neurons. J Neurosci. 2004; 24:7985–7998. [PubMed: 15371499]

Joiner WJ, Friedman EB, Hung HT, Koh K, Sowcik M, Sehgal A, Kelz MB. Genetic and anatomical basis of the barrier separating wakefulness and anesthetic-induced unresponsiveness. PLoS genetics. 2013; 9:e1003605. [PubMed: 24039590]

Kaneko M, Park JH, Cheng Y, Hardin PE, Hall JC. Disruption of synaptic transmission or clock-gene-product oscillations in circadian pacemaker cells of Drosophila cause abnormal behavioral rhythms. J Neurobiol. 2000; 43:207–233. [PubMed: 10842235]

Kudo T, Loh DH, Kuljis D, Constance C, Colwell CS. Fast delayed rectifier potassium current: critical for input and output of the circadian system. J Neurosci. 2011; 31:2746–2755. [PubMed: 21414897]

Kuhlman SJ, McMahon DG. Rhythmic regulation of membrane potential and potassium current persists in SCN neurons in the absence of environmental input. The European journal of neuroscience. 2004; 20:1113–1117. [PubMed: 15305881]

Kuhlman SJ, McMahon DG. Encoding the ins and outs of circadian pacemaking. Journal of biological rhythms. 2006; 21:470–481. [PubMed: 17107937]

Kula-Eversole E, Nagoshi E, Shang Y, Rodriguez J, Allada R, Rosbash M. Surprising gene expression patterns within and between PDF-containing circadian neurons in Drosophila. Proceedings of the National Academy of Sciences of the United States of America. 2010; 107:13497–13502. [PubMed: 20624977]

Kunst M, Hughes ME, Raccuglia D, Felix M, Li M, Barnett G, Duah J, Nitabach MN. Calcitonin gene-related Peptide neurons mediate sleep-specific circadian output in Drosophila. Curr Biol. 2014; 24:2652–2664. [PubMed: 25455031]

Langmead B, Trapnell C, Pop M, Salzberg SL. Ultrafast and memory-efficient alignment of short DNA sequences to the human genome. Genome biology. 2009; 10:R25. [PubMed: 19261174]

Lear BC, Darrah EJ, Aldrich BT, Gebre S, Scott RL, Nash HA, Allada R. UNC79 and UNC80, putative auxiliary subunits of the NARROW ABDOMEN ion channel, are indispensable for robust circadian locomotor rhythms in Drosophila. PLoS One. 2013; 8:e78147. [PubMed: 24223770]

Lear BC, Lin JM, Keath JR, McGill JJ, Raman IM, Allada R. The ion channel narrow abdomen is critical for neural output of the Drosophila circadian pacemaker. Neuron. 2005; 48:965–976. [PubMed: 16364900]

Lee C, Bae K, Edery I. The Drosophila CLOCK protein undergoes daily rhythms in abundance, phosphorylation, and interactions with the PER-TIM complex. Neuron. 1998; 21:857–867. [PubMed: 9808471]

Lu B, Su Y, Das S, Liu J, Xia J, Ren D. The neuronal channel NALCN contributes resting sodium permeability and is required for normal respiratory rhythm. Cell. 2007; 129:371–383. [PubMed: 17448995]

Lu B, Su Y, Das S, Wang H, Wang Y, Liu J, Ren D. Peptide neurotransmitters activate a cation channel complex of NALCN and UNC-80. Nature. 2009; 457:741–744. [PubMed: 19092807]

Meredith AL, Wiler SW, Miller BH, Takahashi JS, Fodor AA, Ruby NF, Aldrich RW. BK calcium-activated potassium channels regulate circadian behavioral rhythms and pacemaker output. Nature neuroscience. 2006; 9:1041–1049. [PubMed: 16845385]

Michel S, Geusz ME, Zaritsky JJ, Block GD. Circadian rhythm in membrane conductance expressed in isolated neurons. Science. 1993; 259:239–241. [PubMed: 8421785]

Michel S, Manivannan K, Zaritsky JJ, Block GD. A delayed rectifier current is modulated by the circadian pacemaker in Bulla. J Biol Rhythms. 1999; 14:141–150. [PubMed: 10194651]

Mohawk JA, Takahashi JS. Cell autonomy and synchrony of suprachiasmatic nucleus circadian oscillators. Trends in neurosciences. 2011; 34:349–358. [PubMed: 21665298]

Nagoshi E, Sugino K, Kula E, Okazaki E, Tachibana T, Nelson S, Rosbash M. Dissecting differential gene expression within the circadian neuronal circuit of Drosophila. Nature neuroscience. 2010; 13:60–68. [PubMed: 19966839]

Nahm SS, Farnell YZ, Griffith W, Earnest DJ. Circadian regulation and function of voltage-dependent calcium channels in the suprachiasmatic nucleus. J Neurosci. 2005; 25:9304–9308. [PubMed: 16207890]

Nash HA, Scott RL, Lear BC, Allada R. An unusual cation channel mediates photic control of locomotion in Drosophila. Curr Biol. 2002; 12:2152–2158. [PubMed: 12498692]

Park D, Griffith LC. Electrophysiological and anatomical characterization of PDF-positive clock neurons in the intact adult Drosophila brain. J Neurophysiol. 2006; 95:3955–3960. [PubMed: 16554503]

Park JH, Helfrich-Forster C, Lee G, Liu L, Rosbash M, Hall JC. Differential regulation of circadian pacemaker output by separate clock genes in Drosophila. Proceedings of the National Academy of Sciences of the United States of America. 2000; 97:3608–3613. [PubMed: 10725392]

Peng Y, Stoleru D, Levine JD, Hall JC, Rosbash M. Drosophila free-running rhythms require intercellular communication. PLoS Biol. 2003; 1:E13. [PubMed: 12975658]

Pennartz CM, de Jeu MT, Bos NP, Schaap J, Geurtsen AM. Diurnal modulation of pacemaker potentials and calcium current in the mammalian circadian clock. Nature. 2002; 416:286–290. [PubMed: 11875398]

Pitts GR, Ohta H, McMahon DG. Daily rhythmicity of large-conductance Ca2+ -activated K+ currents in suprachiasmatic nucleus neurons. Brain research. 2006; 1071:54–62. [PubMed: 16412396]

Raman IM, Gustafson AE, Padgett D. Ionic currents and spontaneous firing in neurons isolated from the cerebellar nuclei. J Neurosci. 2000; 20:9004–9016. [PubMed: 11124976]

Roberts A, Trapnell C, Donaghey J, Rinn JL, Pachter L. Improving RNA-Seq expression estimates by correcting for fragment bias. Genome biology. 2011; 12:R22. [PubMed: 21410973]

Schaap J, Pennartz CM, Meijer JH. Electrophysiology of the circadian pacemaker in mammals. Chronobiology international. 2003; 20:171–188. [PubMed: 12723879]

Seluzicki A, Flourakis M, Kula-Eversole E, Zhang L, Kilman V, Allada R. Dual PDF signaling pathways reset clocks via TIMELESS and acutely excite target neurons to control circadian behavior. PLoS Biol. 2014; 12:e1001810. [PubMed: 24643294]

Shafer OT, Rosbash M, Truman JW. Sequential nuclear accumulation of the clock proteins period and timeless in the pacemaker neurons of Drosophila melanogaster. J Neurosci. 2002; 22:5946–5954. [PubMed: 12122057]

Sheeba V, Gu H, Sharma VK, O'Dowd DK, Holmes TC. Circadian- and light-dependent regulation of resting membrane potential and spontaneous action potential firing of Drosophila circadian pacemaker neurons. J Neurophysiol. 2008; 99:976–988. [PubMed: 18077664]

Sim CK, Forger DB. Modeling the electrophysiology of suprachiasmatic nucleus neurons. J Biol Rhythms. 2007; 22:445–453. [PubMed: 17876065]

Swayne LA, Mezghrani A, Varrault A, Chemin J, Bertrand G, Dalle S, Bourinet E, Lory P, Miller RJ, Nargeot J, et al. The NALCN ion channel is activated by M3 muscarinic receptors in a pancreatic beta-cell line. EMBO reports. 2009; 10:873–880. [PubMed: 19575010]

Tomaiuolo M, Bertram R, Leng G, Tabak J. Models of electrical activity: calibration and prediction testing on the same cell. Biophysical journal. 2012; 103:2021–2032. [PubMed: 23199930]

Xie L, Gao S, Alcaire SM, Aoyagi K, Wang Y, Griffin JK, Stagljar I, Nagamatsu S, Zhen M. NLF-1 delivers a sodium leak channel to regulate neuronal excitability and modulate rhythmic locomotion. Neuron. 2013; 77:1069–1082. [PubMed: 23522043]

Yang Z, Sehgal A. Role of molecular oscillations in generating behavioral rhythms in Drosophila. Neuron. 2001; 29:453–467. [PubMed: 11239435]

Yao Z, Shafer OT. The Drosophila circadian clock is a variably coupled network of multiple peptidergic units. Science. 2014; 343:1516–1520. [PubMed: 24675961]

Zhang L, Chung BY, Lear BC, Kilman VL, Liu Y, Mahesh G, Meissner RA, Hardin PE, Allada R. DN1(p) circadian neurons coordinate acute light and PDF inputs to produce robust daily behavior in Drosophila. Curr Biol. 2010a; 20:591–599. [PubMed: 20362452]

Zhang Y, Liu Y, Bilodeau-Wentworth D, Hardin PE, Emery P. Light and temperature control the contribution of specific DN1 neurons to Drosophila circadian behavior. Curr Biol. 2010b; 20:600–605. [PubMed: 20362449]

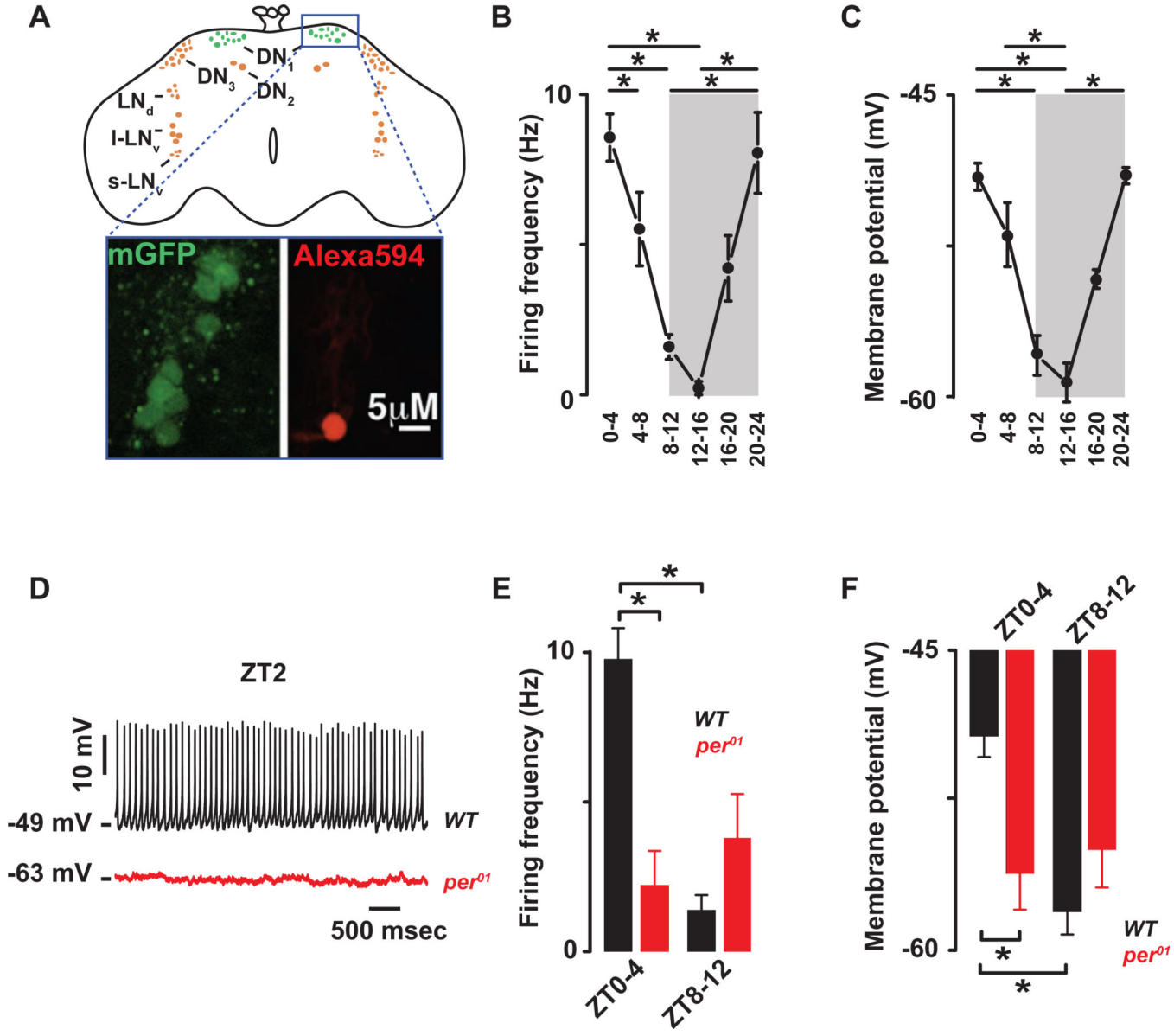

Figure 1. The cellular excitability of the *Drosophila* DN1p circadian pacemaker neurons is clock controlled

(**A**) Schematic and image of the *Drosophila* brain indicating the location of the DN1ps and other clock neurons. Representative images of the GFP-expressing DN1ps in the intact *Drosophila* brain are shown below. The DN1ps were labeled by using the Clk4.1M–G4 driving the expression of U-CD8-GFP. Whole-cell access to GFP labeled neurons was confirmed following diffusion of Alexa Fluor 594 biocytin included in intracellular recording solution. All recorded *WT* neurons are plotted against time of day (in 4 hours bins) to show daily rhythms of firing frequency (**B**) and membrane potential (**C**). Grey areas represent the dark phase of the LD cycle. Asterisks indicate statistical significance ($p<0.05$) from a one-way ANOVA, Tukey's post-hoc test. (**D**) Representative current clamp recordings at Zeitgeber Time-2 (ZT2) showing that the *per*^{01} DN1ps neurons (red) are hyperpolarized and silent compared to *WT* DN1p neurons (black). Histogram showing the

decrease in firing frequency (**E**) and membrane potential (**F**) and lack of daily rhythm in *per*^{01} (red, 2.2±1.1Hz, −56±2 mV, n=15 at ZT0-4 and 3.9±1.5Hz, −55±1.9 mV, n=10 at ZT8–12, p>0.41) when compared to *WT* (black) DN1p neurons. Results are expressed as mean±SEM. Asterisks indicate statistical significance (p<0.05) from t-test performed in *WT* at ZT0-4 *vs* ZT8–12. See also Figures. S.1–2 and Tables S.1–2.

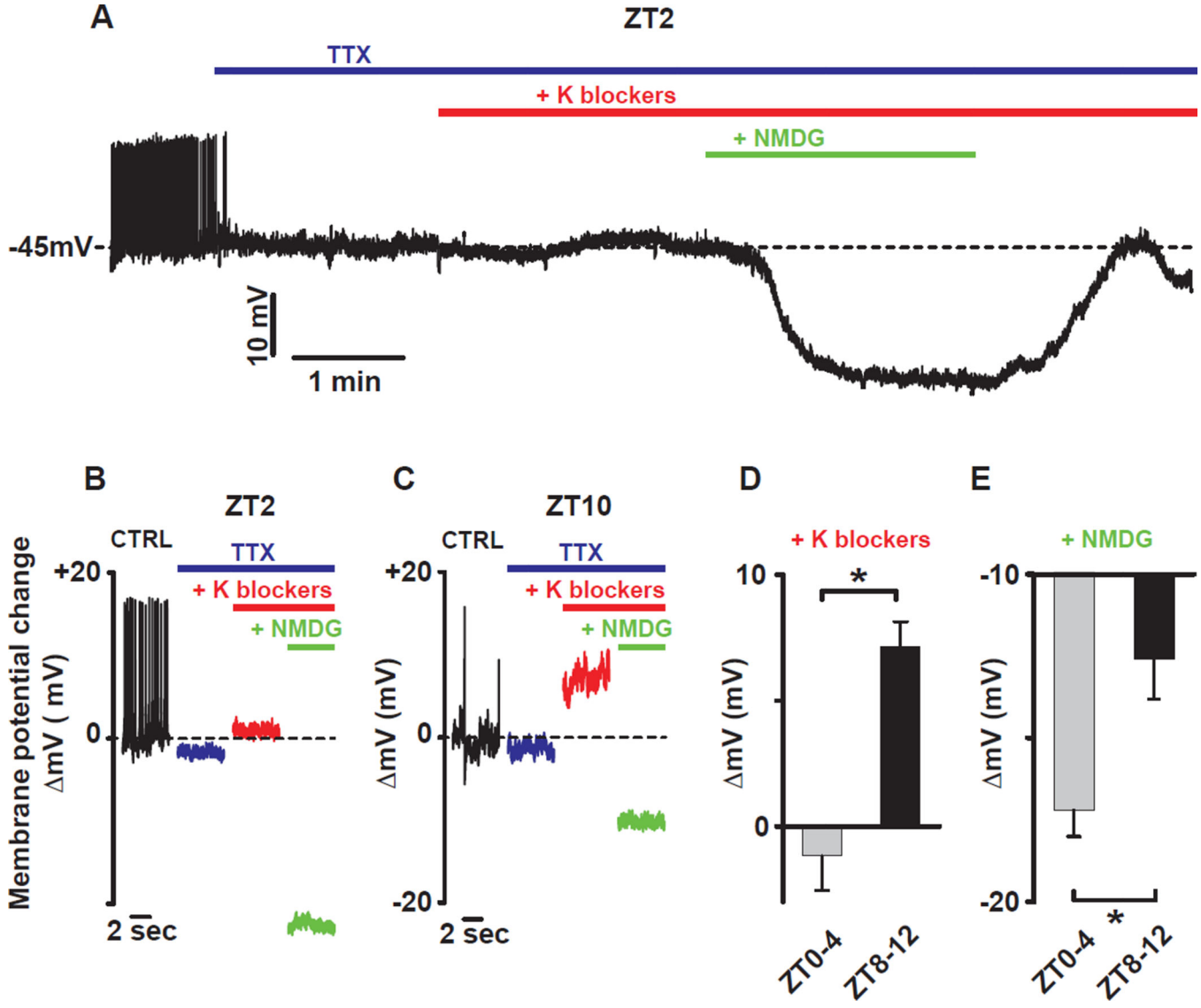

Figure 2. Time of day dependent effects of resting K and sodium leak conductance blockade on membrane potential in DN1p neurons

(**A**) Representative current clamp recording at ZT2 showing the effect of K and sodium conductance blockers on membrane potential. Bars indicate when drugs were applied (blue: TTX 10μM, red: TEA 10mM, 4-AP 5mM, CsCl 2mM and green: NMDG to replace the sodium from the extracellular solution). The effect of K blockers and sodium replacement on the membrane potential at different times of day are shown in (**B**) for ZT2 and (**C**) for ZT10. (**D**) Averaged changes of the membrane potential by K blockers (10mM TEA, 5mM 4-AP and 2mM CsCl): −1.2±1.4mV, n=5 between ZT0-4 and 7.1±1mV, n=5 between ZT8–12 and (**E**) sodium replacement with NMDG: −17.2±0.8mV, n=5 between ZT0-4 and −12.6±1.2mV, n=5 between ZT8–12. Results are expressed as mean±SEM. Asterisks indicate statistical significance ($p<0.05$) from t-test.

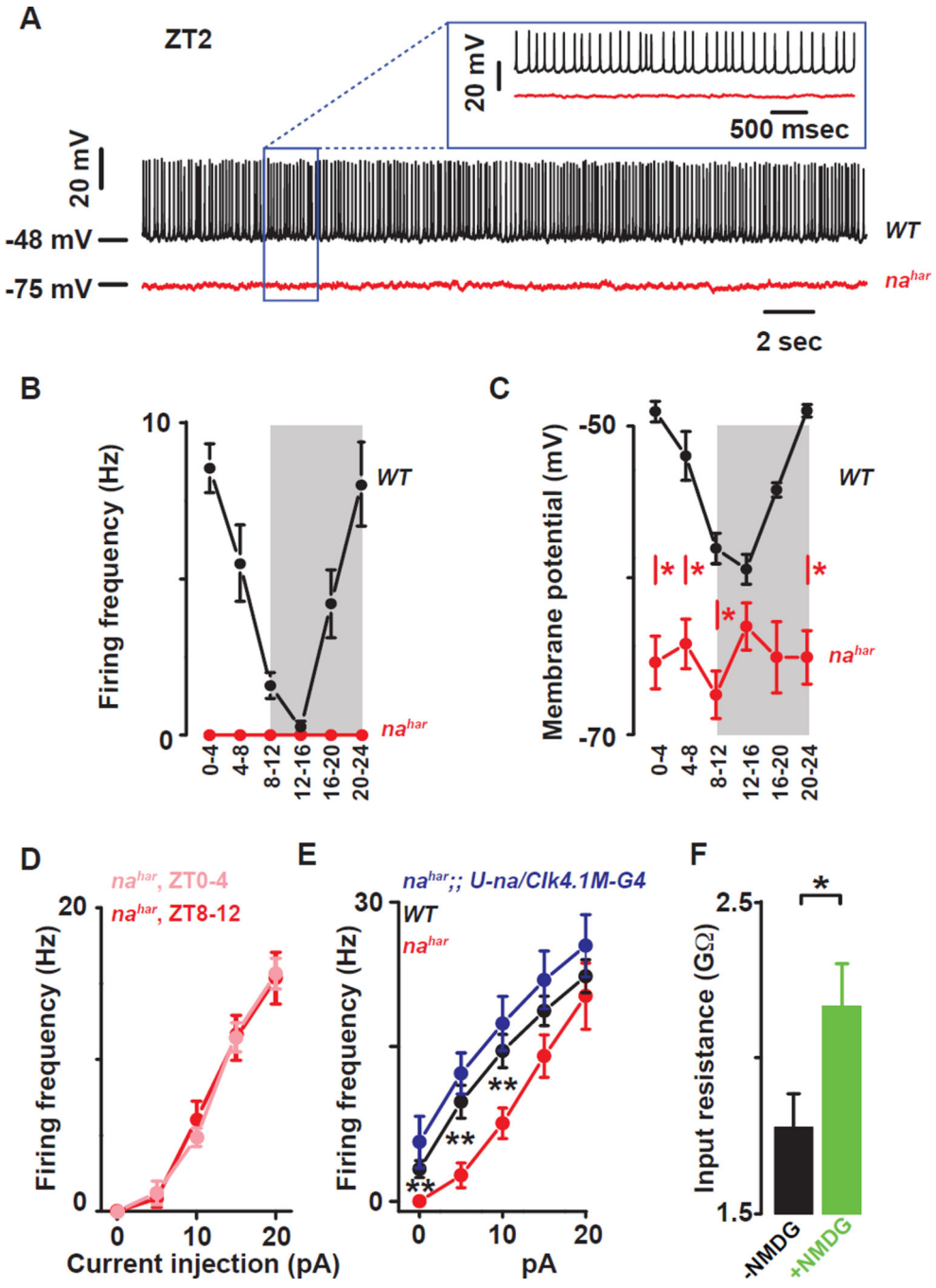

Figure 3. The ion channel NARROW ABDOMEN controls *Drosophila* circadian pacemaker neuronal rhythms

(**A**) Representative current clamp recordings at ZT2 showing that the *na*^{har} DN1ps neurons (red) are hyperpolarized and silent compared to *WT* DN1p neurons (black). Statistical analysis comparing the firing frequency (**B**) and membrane potential (**C**) of the *WT* (black) and *na*^{har} (red) DN1p neurons. Red asterisks indicate statistical significance between *WT* and *na*^{har} neurons ($p<0.05$, from a one-way ANOVA, Tukey's post-hoc test). (Data for *WT* neurons are also depicted in Fig 1B and 1C). (**D**) Depolarizing current injections confirm the

lack of detectable rhythms in cellular excitability in the na^{har} neurons (light red: ZT0-4, dark red ZT8–12, $p>0.35$). (**E**) The decrease in cellular excitability can be restored by rescuing the expression of NA only in the DN1p in the mutant: *WT* (black), na^{har} (red) and na^{har};; *U-na/Clk4.1M–G4* (blue) DN1ps neurons. (**F**) Histograms showing that sodium substitution with NMDG induces an increase in the input resistance indicating that NA is open at rest (black and green columns are before and after NMDG substitution, respectively). Results are expressed as mean±SEM. Asterisks indicate statistical significance (t-test, $p<0.05$). See also Tables S.1–2.

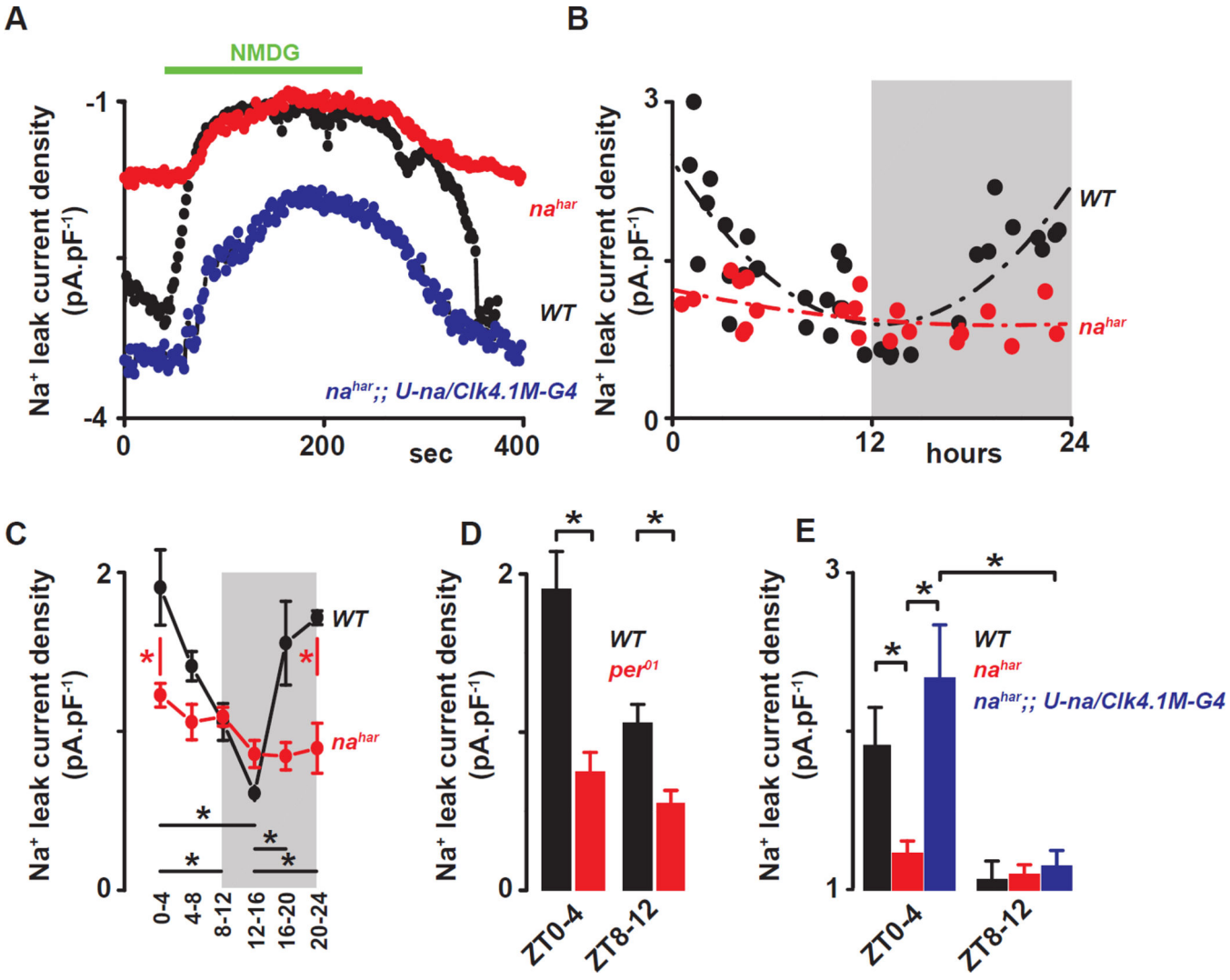

Figure 4. The sodium leak current is under clock control in *Drosophila* circadian pacemaker neurons

(**A**) Representative time courses showing the sodium leak current (I_{NA}) recorded at −113mV from a ramp protocol in *WT* (black), *na*^{har} (red) and *na*^{har}*;; U-na/Clk4.1M–G4* (blue) DN1p neurons. (**B**) All recorded *WT* neurons (black dots) and *na*^{har} neurons (red dots) are plotted against time of day for sodium leak current (I_{NA}). (**C**) Quantification and statistical analysis are shown. Grey areas represent the dark phase of the LD cycle. Red asterisks indicate statistical significance between *WT* and *na*^{har} neurons, and black asterisks indicate statistical significance between different time points in *WT* neurons ($p<0.05$) from a one-way ANOVA, Tukey's post-hoc test. (**D**) Histograms showing the NA current in *WT* (black) and *per*^{01} (red) DN1ps recorded at different times of day ZT0-4 *vs* ZT8–12 (for *per*^{01}, $I_{NA}=0.7\pm0.2 pA.pF^{-1}$, n=8 at ZT0-4 and $0.5\pm0.1 pA.pF^{-1}$, n=7 at ZT8–12. Asterisks indicate statistical difference between *WT* and *per*^{01}, $p<0.05$ from t-test). (**E**) Histograms showing the sodium leak current in *WT* (black), *na*^{har} (red) and *na*^{har}*;; U-na/Clk4.1M–G4* (blue) DN1p neurons at different times of day (ZT0-4 *vs* ZT8–12) (for *na*^{har}*;; U-na/Clk4.1M–G4*,

I_{NA}=2.3±0.3pA.pF^{-1}, n=4 at ZT0-4 and 1.1±0.1pA.pF^{-1}, n=4 at ZT8–12). Results are expressed as mean±SEM. Asterisks indicate statistical significance ($p<0.05$) from a t-test.

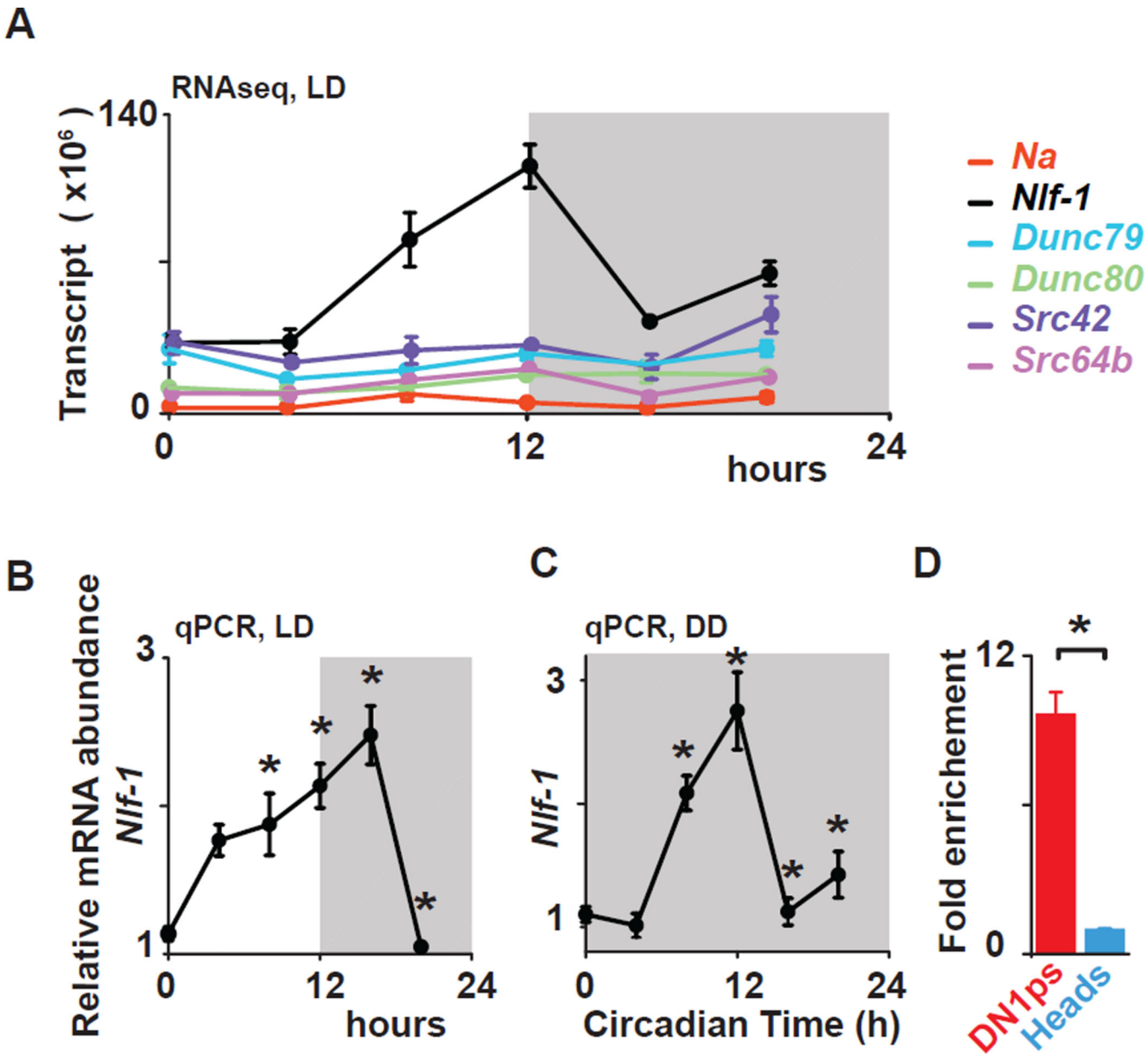

Figure 5. *Nlf-1* is rhythmically expressed in DN1p neurons

(**A**) *Nlf-1* mRNA shows rhythmic expression using RNA-seq data from FACS sorted DN1p neurons in LD (for isoform RB- shown in graph, BH corrected p=0.005). *na*, *Unc79*, *Unc80*, *Src64B*, and *Src42a* are not robustly cycling (graph shows isoforms with highest expression : BH= 0.28 for *na-RF*, 0.2 for *Dunc79-RE*, 0.85 for *Dunc80-RE*, 0.71 for *Src42a–RA* and 0.07 for *Src64B–RJ*). *Nlf-1* cycles under LD (**B**) and during the first day of constant darkness (DD1) conditions (**C**) in DN1ps using qPCR. Based on two independent experiments, an asterisk indicates differences statistically significant one-way ANOVA, Tukey's post-hoc test, LD ZT0 *vs* ZT12 p= 0.0011, ZT0 *vs* ZT16, p= 0.000142, ZT4 *vs* ZT16 p=0.029, ZT0 *vs* ZT8 p=0.022, ZT12 *vs* ZT20, p= 0.000441, ZT16 *vs* ZT20 p= 0.000136. DD1 CT0 *vs* CT8 p= 0.01081, CT0 *vs* CT12 p= 0.000142, CT12 *vs* CT16 p=

0.000145 and CT12 *vs* CT20 p= 0.000459. (**D**) *Nlf-1* expression is enriched in the DN1ps *vs* whole head (t-test, $p<0.02$). Results are expressed as mean±SEM.

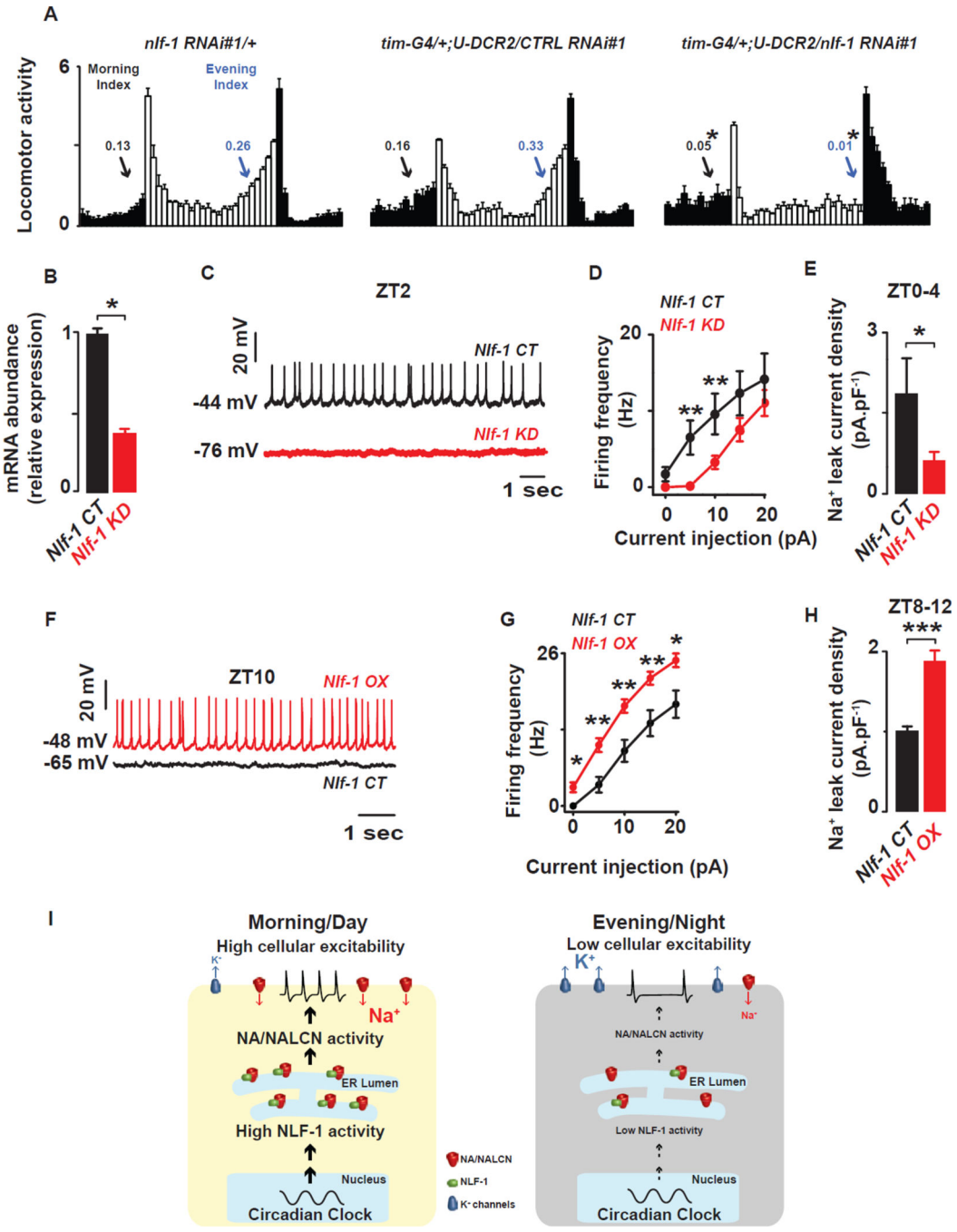

Figure 6. ***Nlf-1*** **is required for anticipatory behavior and NA current**

(**A**) *Nlf-1* RNAi expressing flies (*tim-G4/+; U-Dcr2/Nlf-1 RNAi#1*) show reduced morning anticipation (Morning Index) and evening anticipation (Evening Index) under LD conditions when compared to genetic controls (*Nlf-1 RNAi#1/+* and *tim-G4/+; U-Dcr2/CTRL RNAi#1*), (t-test, $p<0.05$). (**B**) *Nlf-1* expression is reduced in the DN1ps of *Nlf-1* RNAi expressing flies (t-test, $p<0.05$) (**C**) Representative current clamp recordings at ZT2 showing that the *Nlf-1* knockdown DN1p neurons (red) are hyperpolarized and silent compared to control DN1p neurons (black). (**D**) Depolarizing current injections confirm the decrease in cellular

excitability in *Nlf-1* knockdown neurons (red) *vs* control (black) ($p<0.05$). (**E**) Sodium leak current density is dramatically reduced in the *Nlf-1* knockdown neurons (red) *vs* control neurons (black) ($1.9\pm0.7 pA.pF^{-1}$, n=4 in *Nlf-1 CT* and $0.6\pm0.2 pA.pF^{-1}$, n=5 in *Nlf-1 KD*, measured at ZT0-4, $p<0.05$). (**F**) Representative current clamp recordings at ZT10 showing that the *Nlf-1* overexpressing DN1p neurons (red) are depolarized and more active compared to control DN1p neurons (black). (**G**) Depolarizing current injections confirm the increase in cellular excitability in *Nlf-1*^{V5} overexpressing neurons (red) *vs* control (black) ($p<0.05$). (**H**) Sodium leak current density is also increased in the *Nlf-1*^{V5} overexpressing neurons (red) *vs* control neurons (black) ($1\pm0.05 pA.pF^{-1}$, n=4 in *Nlf-1 CT* and $1.9\pm0.1 pA.pF^{-1}$, n=5 in *Nlf-1 OX*, measured at ZT8–12, $p<0.05$). Results are expressed as mean±SEM. Asterisks indicate statistical significance ($p<0.05$ from a t-test). A summary cartoon depicting the conserved bicycle model for controlling membrane excitability of circadian pacemaker neurons is shown in (**I**). In the morning/day, the molecular clock drives high NLF-1 activity increasing the sodium leak activity and K conductances are reduced thus increasing cellular excitability. In the evening/night, the sodium leak is decreased and, in parallel, K conductances are high, thus silencing the neurons. This dual regulation of the conductances responsible for the membrane properties is critical for driving high amplitude rhythmic oscillations of cellular excitability. See also Figures. S.3–5 and Tables S.2–4.

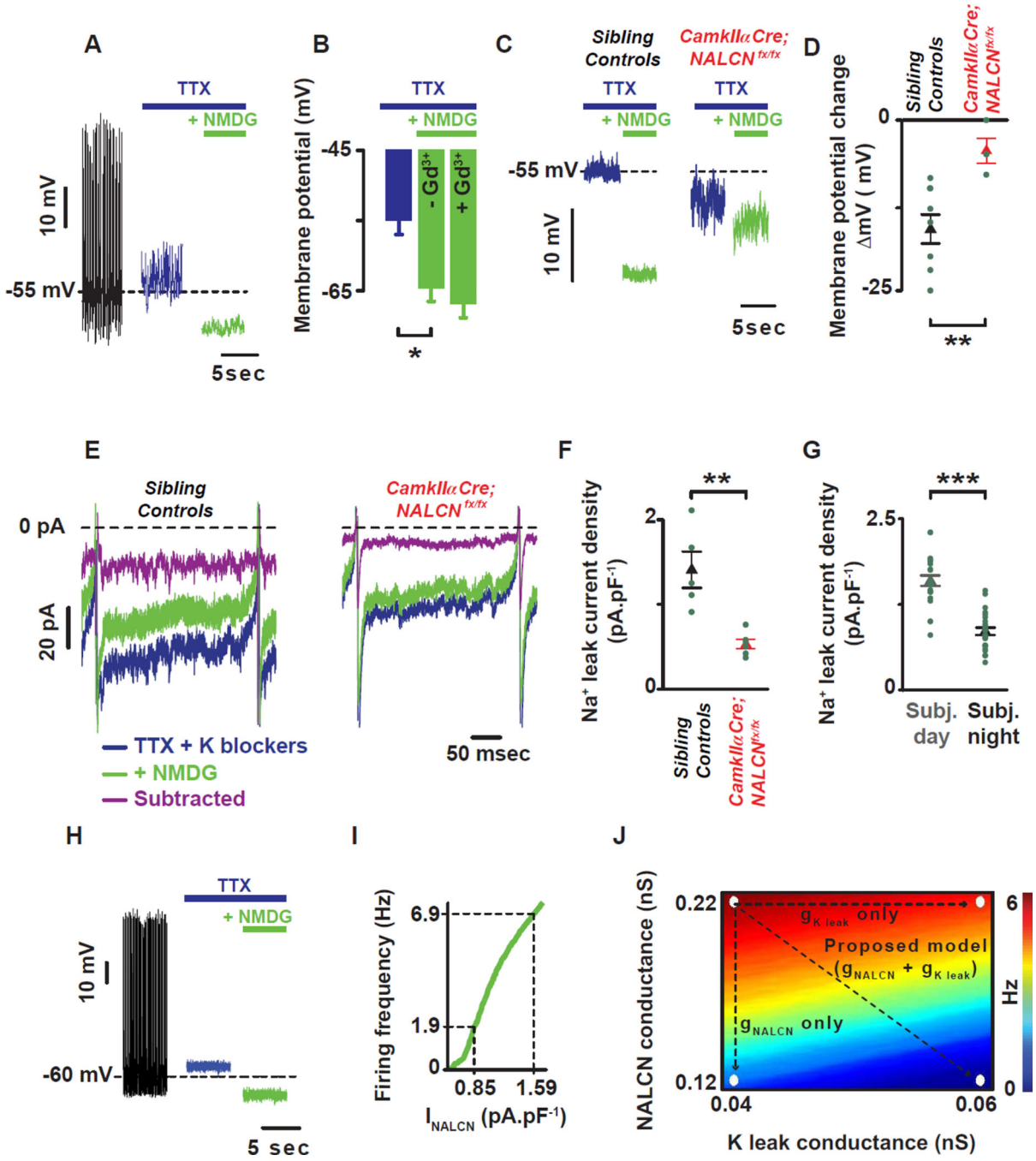

Figure 7. NALCN current is under clock control in mammalian SCN pacemaker neurons

(**A**) Representative current clamp recording showing the role of the TTX-resistant sodium leak (difference between green and blue) in setting the membrane potential of mammalian SCN neurons. (**B**) NMDG hyperpolarizes the cell with no additional effect in the presence of Gd^{3+}. (**C**) NMDG-evoked hyperpolarization was reduced in a brain specific knockout of NALCN. (**D**) Quantification and statistical analysis of the NMDG-evoked hyperpolarization are shown: −15.9±2.0mV, n=9 in controls (black triangle) and −4.5±1.7mV, n=4 (red triangle). Asterisks indicate statistical significance (t-test, p=0.005). (**E**) Action potential

clamp recordings showing the sodium leak flowing during the interspike interval in SCN neurons from sibling control (left) and *CamkIIa-Cre;NALCN*$^{fx/fx}$ animals (right). In the presence of TTX and K blockers (blue trace), the sodium leak current flowing during the interspike interval (I_{NALCN}) was reduced after sodium substitution with NMDG (green trace). The sodium leak current (I_{NALCN} = subtracted = purple trace) was revealed by subtracting the inward current in the presence of NMDG from the inward current present with TTX and K blockers. (**F**) I_{NALCN} was reduced in *CamkIIa-Cre;NALCN*$^{fx/fx}$ compared to sibling controls animals (0.5±0.1pA.pF^{-1}, n=6 in *CamkIIa-Cre;NALCN*$^{fx/fx}$ (red triangle) and 1.4±0.2pA.pF^{-1}, n=5 in sibling controls (black triangle)). Asterisks indicate statistical significance (t-test, p=0.002). (**G**) Circadian variation of I_{NALCN}: 1.6±0.1pA.pF^{-1}, n=25 during the subjective day (grey columns) and 0.8±0.1pA.pF^{-1}, n=23 during the subjective night (black columns). Asterisks indicate statistical significance (t-test, p<0.001). Green dots represent individual cells. (**H**) Simulations showing the role of TTX resistant sodium leak in setting the membrane potential using a mathematical model of SCN membrane excitability. Voltage traces from control simulation (g_{Na} = 229 nS, g_{NALCN} = 0.22 nS) and simulated application of TTX (g_{Na} = 0 nS) and NMDG (g_{NALCN} = 0 nS). (**I**) The model predicts the magnitude of change in firing rate as a function of magnitude of change in NALCN current density (g_{NALCN} = 0.12 to 0.22 nS). A decrease of 0.74 pA.pF^{-1} in I_{NALCN} (observed between the subjective day and night (**G**)) leads to a 5 Hz decrease in firing rate. (**J**) Firing rate as a function of g_{NALCN} and g_{Kleak} in a model SCN neuron. Arrows: decreasing g_{NALCN} alone reduces firing rate from 7 Hz to 2 Hz, whereas increasing g_{Kleak} reduces firing rate from 7 Hz to 6 Hz. Concurrently decreasing g_{NALCN} and increasing g_{Kleak} reduces firing rate from 7 Hz to 0.5 Hz. Results are expressed as mean±SEM. See also Figures. S.6–7.